CNWRA *A center of excellence in earth sciences and engineering*

A Division of Southwest Research Institute™
6220 Culebra Road • San Antonio, Texas, U.S.A. 78228-5166
(210) 522-5160 • Fax (210) 522-5155

March 14, 2002
Contract No. NRC–02–97–009

U.S. Nuclear Regulatory Commission
ATTN: Mrs. Deborah A. DeMarco
Office of Nuclear Material Safety and Safeguards
TWFN Mail Stop 8 A23
Washington, DC 20555

Subject: Transmission of Posters: (1) Relay Ramp Style in Massive Limestone: Examples from the Sierra Del Carmen, West Texas, (2) Influence of Regional Strains in the Development of Faulted Domes in the Offshore Middle East, (3) Estimation of Sub-Seismic Fault Populations

Dear Mrs. DeMarco:

Attached are three posters for presentation at the American Association of Petroleum Geologists (AAPG) 2002 National Meeting. The structural concepts described in these posters resulted from work done for Japan National Oil Corporation. These concepts have given CNWRA staff a broader understanding of normal faulting processes, such as those that occurred at Yucca Mountain. The posters are sent for information only, and costs for presenting these posters will not be incurred by NRC.

Should you have any questions regarding this, please contact Dr. David Ferrill at (210) 522-6082 or Dr. H. Lawrence McKague at (210) 522-5183.

Sincerely,

Budhi Sagar
Technical Director

HLM:rae

Attachment

cc: J. Linehan, W. Reamer, B. Leslie, E. Whitt, B. Meehan, D. Brooks, J. Greeves, J. Schlueter, S. Wastler, T. Essig, K. Stablein, P. Justus, J. Trapp, W. Patrick, CNWRA Dirs/EMs, D. Ferrill, D. Sims, J. Stamatakos, D. Waiting, T. Nagy (SwRI Contracts), A. Morris

D:\GLGP Group\letters\misc\posters-03-14-2002bs.wpd

Washington Office • Twinbrook Metro Plaza #210
12300 Twinbrook Parkway • Rockville, Maryland 20852-1606

RELAY RAMP STYLE IN MASSIVE LIMESTONE: EXAMPLES FROM THE SIERRA DEL CARMEN, WEST TEXAS

David A. Ferrill[1], Alan P. Morris[2], Deborah J. Waiting[1], Futoshi Tsuneyama[3], Yoshihiko Tamura[4],and Darrell W. Sims[1]

[1]CNWRA, Southwest Research Institute, 6220 Culebra Road, San Antonio, Texas 78238-5166, USA

[2]Department of Earth and Environmental Science, University of Texas at San Antonio, San Antonio, Texas 78249-0663, USA

[3]Technology Research Center, Japan National Oil Corporation, Mihamaku, Chiba, 261-0025, Japan

[4]Geoscience Group Technical Department Japan Oil Development Co., Ltd., Kayabacho Tower 21-2 Shinkawa 1-Chome Chuo-ku, Tokyo 104-0033, Japan

Panel 1 of 3

Introduction

Relay ramps and breached relay ramps are important locations of enhanced permeability in fractured reservoirs.

The spectrum of relay ramp geometries includes relay ramps where displacement is partially accommodated by development of synthetic dip or several parallel normal faults within the relay ramp.

Relay ramps that accommodate fault system displacement by development of synthetic dip or smaller scale faulting are recognizable as displacement minima on cumulative displacement profiles of the bounding faults.

The Sierra Del Carmen in west Texas provides excellent exposure of a normal fault system in the thick, massive Cretaceous Santa Elena Limestone.

- **Displacement maxima are on the order of tens to hundreds of meters and are in the size range of structures resolvable using seismic methods.**

- **Fault linkage developed by curved lateral propagation of overlapping fault tips is common, while fault linkage by connecting fault formation is rare or absent.**

- **Detailed analysis of relay ramps in various stages of development shows that relay ramps commonly contain smaller displacement normal faults parallel or at a low angle to the bounding faults, producing nested relay ramps.**

- **In each case, these relay ramps correspond to displacement minima on cumulative displacement profiles of the bounding faults.**

- **This relay ramp style may reflect early distributed faulting between underlapping faults.**

Prediction of analogous subseismic faults in production settings may be possible by identifying displacement minima on cumulative displacement profiles of seismically imaged faults.

Styles of Relay Ramp Geometry in Normal Fault Systems

(a)

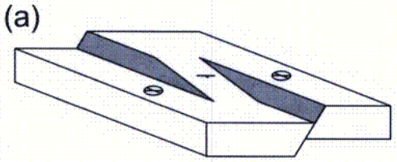

Ideal relay ramp where all displacement is accommodated by fault slip and displacement transfer is accomplished by fault-parallel dip in the relay ramp.

(b)

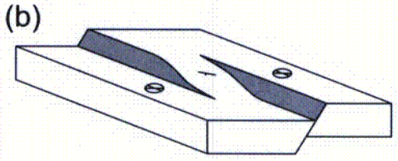

Relay ramp where displacement transfer is partially accomplished by synthetic dip development in the relay ramp.

(c)

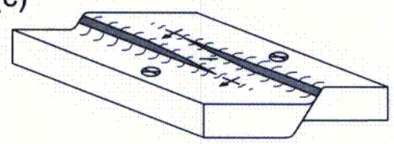

Monoclinal folding ahead of fault tip lines produces synthetic dip panels that accomplish component of fault system displacement.

(d)

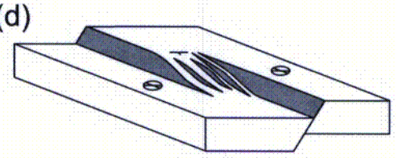

Development of several parallel faults in relay system that produces nested relay ramps (relay ramps within a relay ramp).

(e)

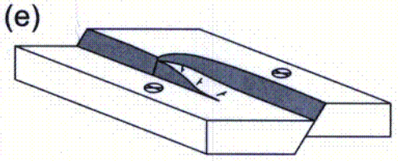

Breakthrough by curved lateral fault propagation. Displacement transfer accomplished by a combination of relay ramp tilting and linked fault displacement.

(f)

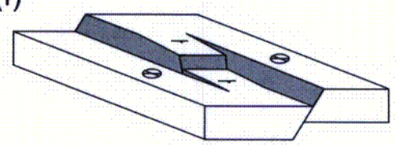

Breakthrough by connecting fault formation. Displacement transfer first by relay ramp development, then by connecting fault across the relay ramp.

Sierra Del Carmen, Texas

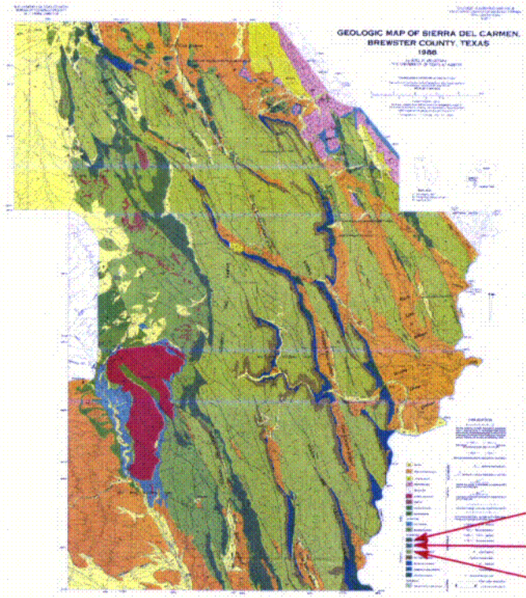

Mountain range along eastern margin of Big Bend National Park, and the contiguous western part of Black Gap Wildlife Management area.

Excellent exposure of normal fault system developed in thick, massive Cretaceous Santa Elena Limestone, exhumed by erosion of the overlying Del Rio Clay.

Fault displacement maxima on the order of tens to hundreds of meters.

Buda Limestone
Del Rio Clay
Santa Elena Limestone

C01

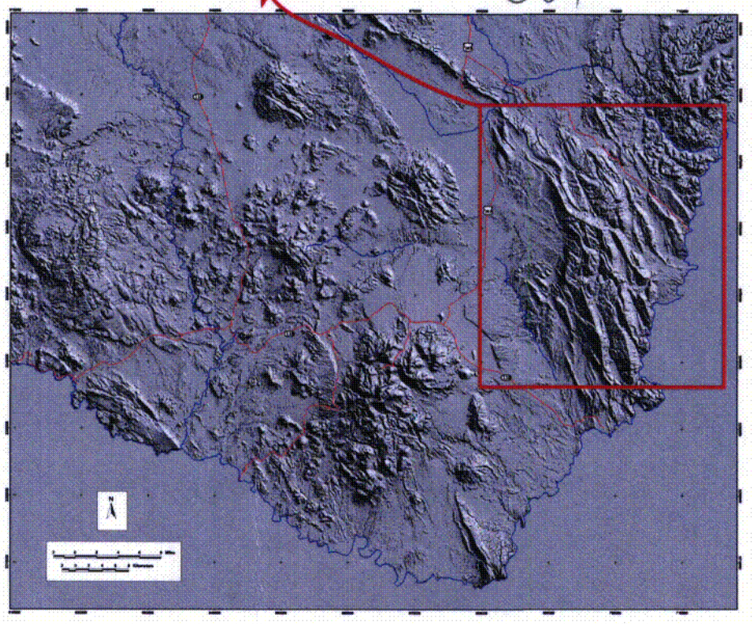

RELAY RAMP STYLE IN MASSIVE LIMESTONE: EXAMPLES FROM THE SIERRA DEL CARMEN, WEST TEXAS

David A. Ferrill[1], Alan P. Morris[2], Deborah J. Waiting[1], Futoshi Tsuneyama[3], Yoshihiko Tamura[4],and Darrell W. Sims[1]

[1]CNWRA, Southwest Research Institute, 6220 Culebra Road, San Antonio, Texas 78238-5166, USA

[2]Department of Earth and Environmental Science, University of Texas at San Antonio, San Antonio, Texas 78249-0663, USA

[3]Technology Research Center, Japan National Oil Corporation, Mihamaku, Chiba, 261-0025, Japan

[4]Geoscience Group Technical Department Japan Oil Development Co., Ltd., Kayabacho Tower 21-2 Shinkawa 1-Chome Chuo-ku, Tokyo 104-0033, Japan

Panel 2 of 3

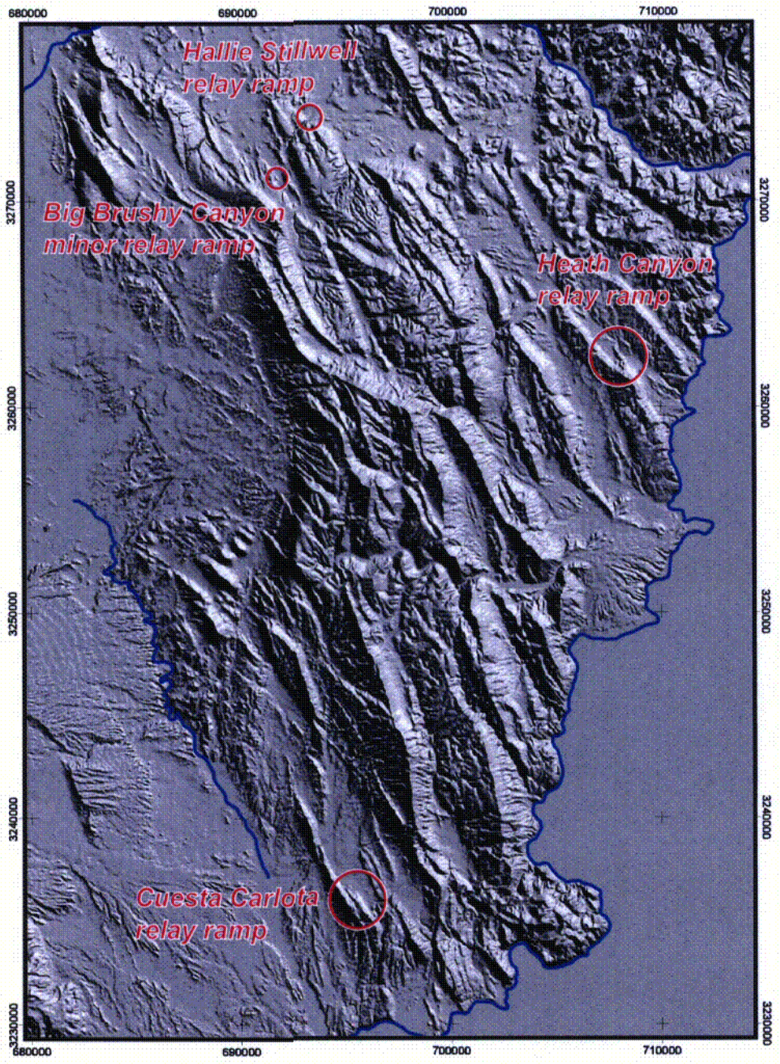

Example 1: Big Brushy Canyon Monocline and Minor Relay Ramp

Fault displacement in massive Santa Elena Limestone is attenuated by the overlying Del Rio Clay so that displacement at the Buda Limestone level is accommodated by formation of a monocline.

Minor breached relay ramp between two left-stepping normal faults. Breached ramp is attached to footwall. Relict fault tip in the footwall and geometry of the breached relay ramp are consistent with fault linkage by curved lateral propagation along the ultimate downthrown trace.

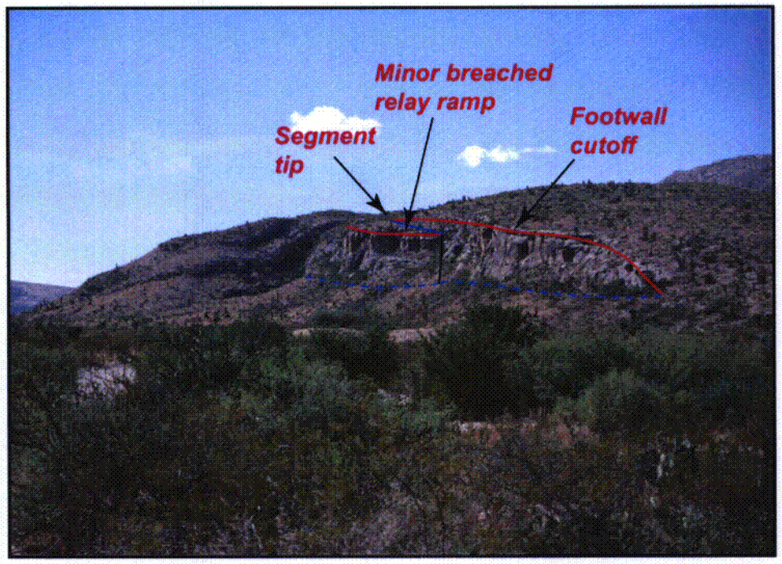

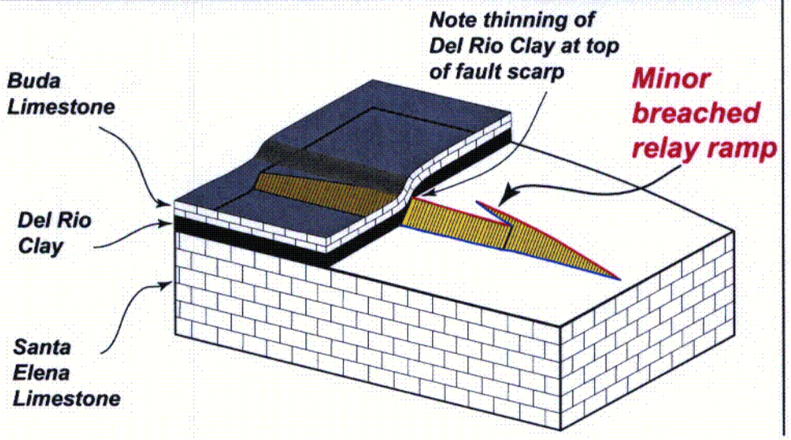

Example 2: Hallie Stillwell Relay Ramp

Intact relay ramp between two left-stepping faults.

Significant synthetic component of bedding dip within relay ramp.

Thus, fault system displacement accomplised by fault displacement and basinward tilting in the ramp

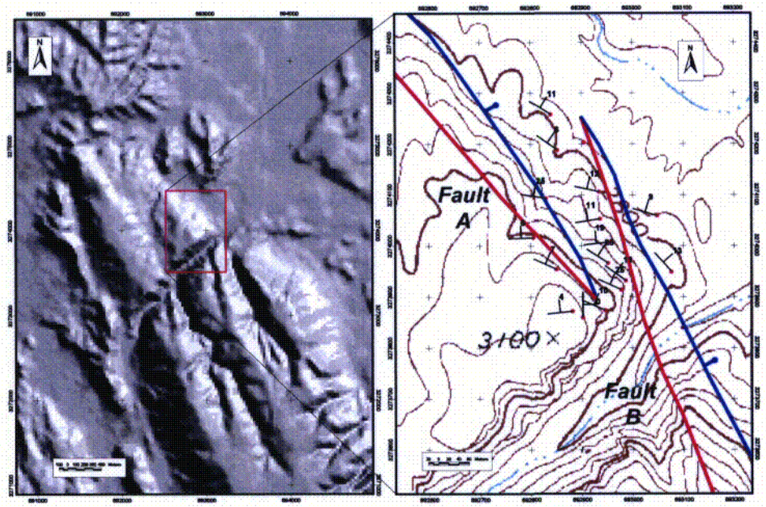

CO2

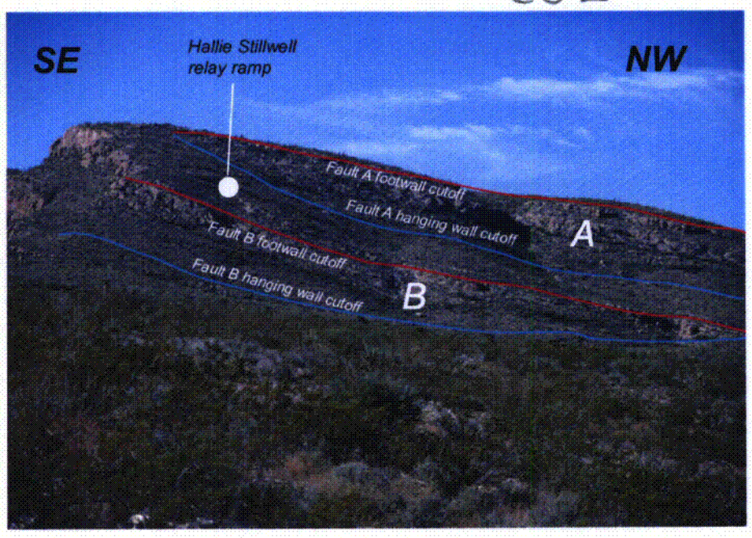

RELAY RAMP STYLE IN MASSIVE LIMESTONE: EXAMPLES FROM THE SIERRA DEL CARMEN, WEST TEXAS

David A. Ferrill[1], Alan P. Morris[2], Deborah J. Waiting[1], Futoshi Tsuneyama[3], Yoshihiko Tamura[4],and Darrell W. Sims[1]

[1]CNWRA, Southwest Research Institute, 6220 Culebra Road, San Antonio, Texas 78238-5166, USA

[2]Department of Earth and Environmental Science, University of Texas at San Antonio, San Antonio, Texas 78249-0663, USA

[3]Technology Research Center, Japan National Oil Corporation, Mihamaku, Chiba, 261-0025, Japan

[4]Geoscience Group Technical Department Japan Oil Development Co., Ltd., Kayabacho Tower 21-2 Shinkawa 1-Chome Chuo-ku, Tokyo 104-0033, Japan

Panel 3 of 3

Example 3: Heath Canyon Relay Ramp

Breached relay ramp between two left-stepping overlapping faults.

Fault connection developed by curved lateral propagation of the SE tip of Fault "A" until intersection with Fault "B" occurred. (Line of intersection is labeled as Branch Line in figures.)

Cuspate footwall geometry.

Seven smaller faults present along northeastern edge of relay ramp. Faults are oblique to bounding faults.

Bedding dips in the ramp are steepest near its updip end, and are progressivley more gentle toward the NW.

Bedding dip has significant antithetic component near the updip end of ramp.

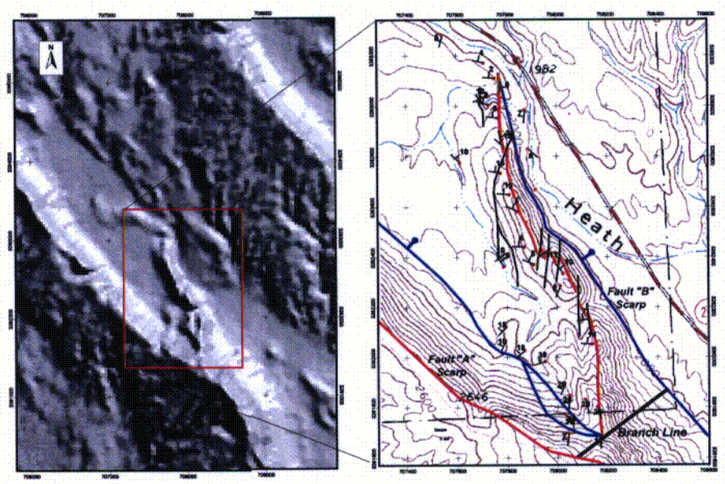

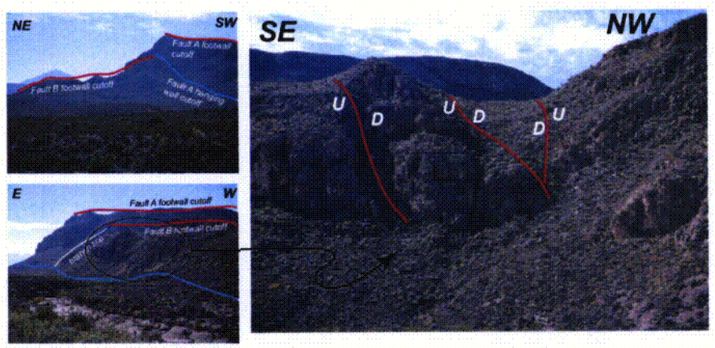

Example 4: Cuesta Carlota Relay Ramp

Intact relay ramp between two left-stepping overlapping northeast dipping normal faults.

In detail, consists of system of nested relay ramps represetned by six faults.

Major faults that define ramp have en echelon segments (separated by smaller relay ramps) at their overlapping tips.

Steepest fault dips are within the nested second order relay ramps.

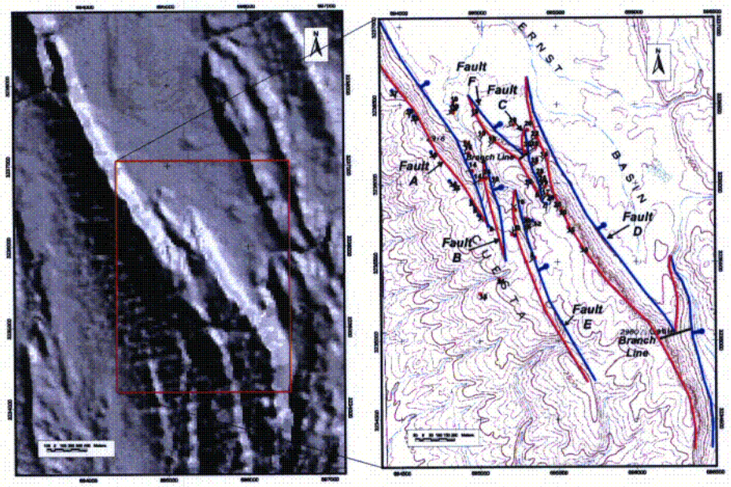

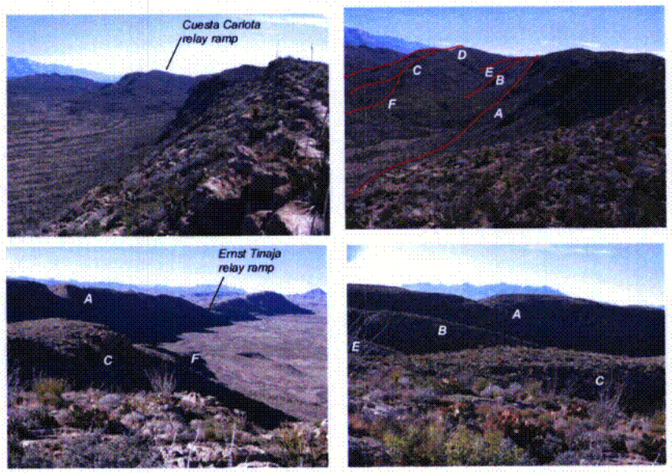

Summary

Relay ramps and breached relay ramps in Santa Elena Limestone of the Sierra Del Carmen display both synthetic and antithetic dip components.

Relay ramps correspond to displacement minima on major bounding faults.

Fault linkage tends to occur by curved lateral propagation of one of the overlapping fault tips.

Connecting faults are uncommon (or absent) in Sierra Del Carmen.

Locally intense deformation manifest by smaller scale faulting and steep layer dips characteristic of relay ramps in Santa Elena Limestone.

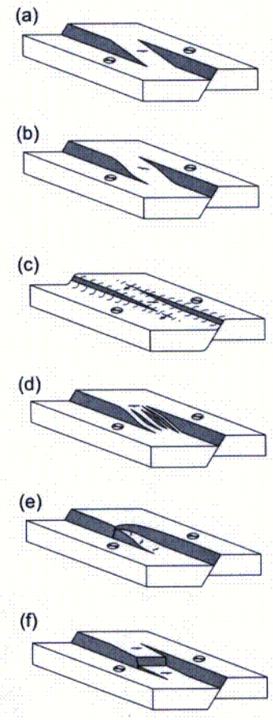

Geometry seen in Santa Elena Limestone?

Yes

Yes

No, but probable in Buda Limestone

Yes

Yes

No

C03

***Acknowledgements:** This work was funded by the Japan National Oil Corporation. We thank Michael T. Pittman (Area Manager) and Texas Parks and Wildlife, Black Gap Wildlife Management Area for permitting us access for field work.*

INFLUENCE OF REGIONAL STRAINS IN THE DEVELOPMENT OF FAULTED DOMES IN THE OFFSHORE MIDDLE EAST

Darrell W. Sims[1], David A. Ferrill[1], Alan P. Morris[2], Deborah J. Waiting[1], Futoshi Tsuneyama[3], Yoshihiko Tamura[4], and Hitoshi Okamura[3]
[1]CNWRA, Southwest Research Institute, 6220 Culebra Road, San Antonio, TX 78238-5166, USA
[2]Department of Earth and Environmental Science, University of Texas, San Antonio, TX 78249, USA
[3]Technology Research Center, Japan National Oil Corporation, Mihama-ku, Chiba 261-0025, Japan
[4]Geoscience Group Technical Department Japan Oil Development Co., Ltd., Kayabacho Tower 21-2 Shinkawa 1-Chome Chuo-ku, Tokyo 104-0033, Japan

Panel 1 of 3

INTRODUCTION

Many oil fields in the offshore Middle East have traps in broad domes developed over salt. A recent 3D seismic survey from a fractured Cretaceous carbonate reservoir reveals that one elliptical dome is cut by an array of parallel normal faults with strike oriented oblique (68°) to the long axis of the elliptical dome. We used clay cake models to

- simulate development of the fault pattern

- understand the relationship between the fault pattern and stress regime.

- simulate the relationship between fault populations mapped using seismic methods and fault populations that seismic methods may not detect.

Our models of dome formation simulated a range of regional strain configurations relative to dome shape and orientation. Fault patterns interpreted from 3D seismic data correlate well with fault patterns developed in models that simulate a regional extension.

Model of elliptical dome formation with preceeding and concurrent regional extension

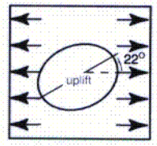

Overview of model configuration

Model 19MAR01

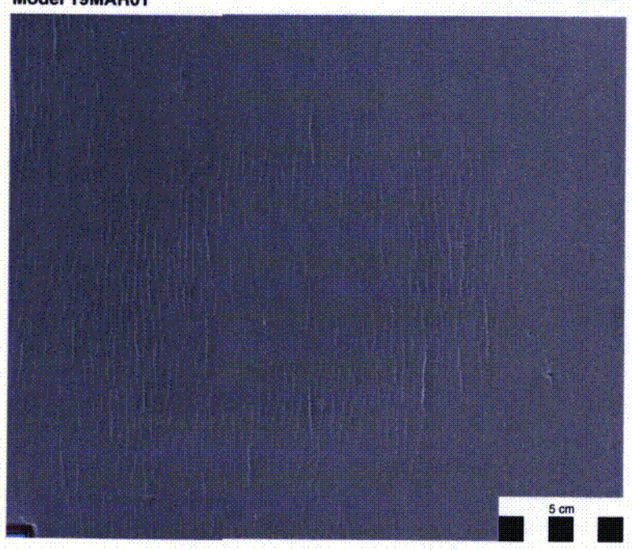

Vertical view of model after 3 cm horizontal regional extension and immediately prior to the initiation of doming. Illumination is from upper and lower right.

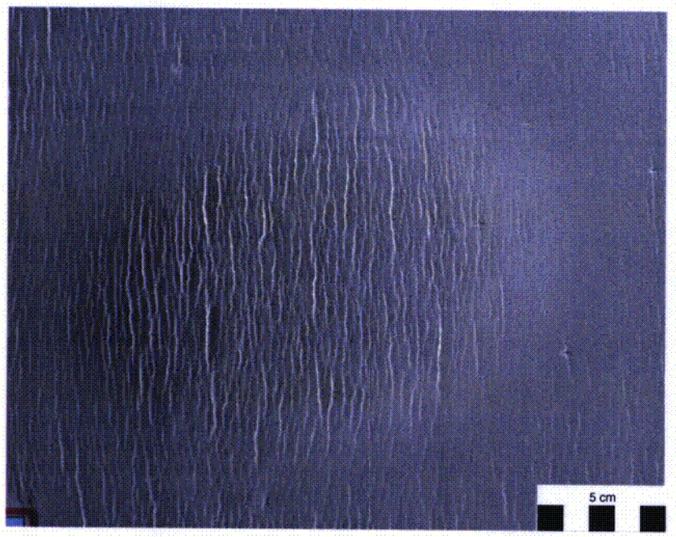

Detail of dome after 4.8 cm horizontal regional extension. Uplift at dome culmination is 0.6 cm. Illumination is from upper and lower right.

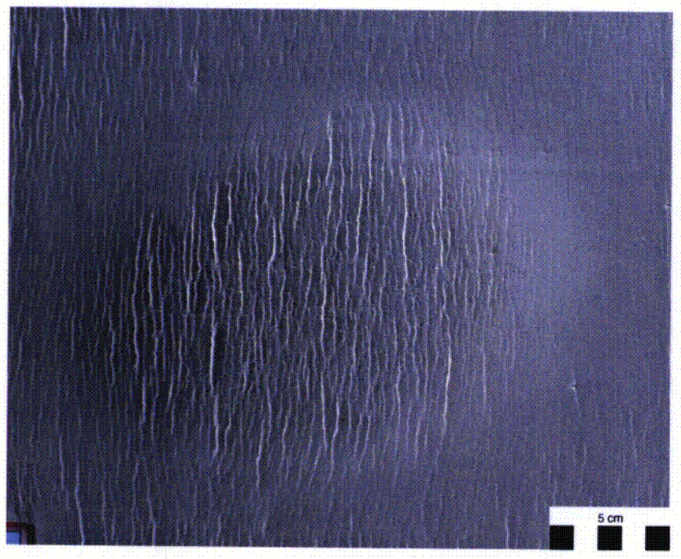

Detail of dome after 5.4 cm horizontal regional extension. Uplift at dome culmination is 0.8 cm. Illumination is from upper and lower right.

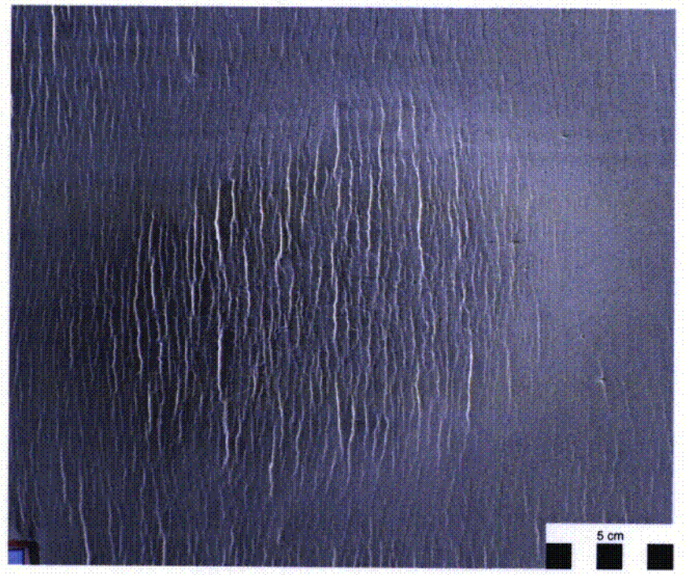

Detail of dome after 5.5 cm horizontal regional extension. Uplift at dome culmination is 0.83 cm. Illumination is from upper and lower right.

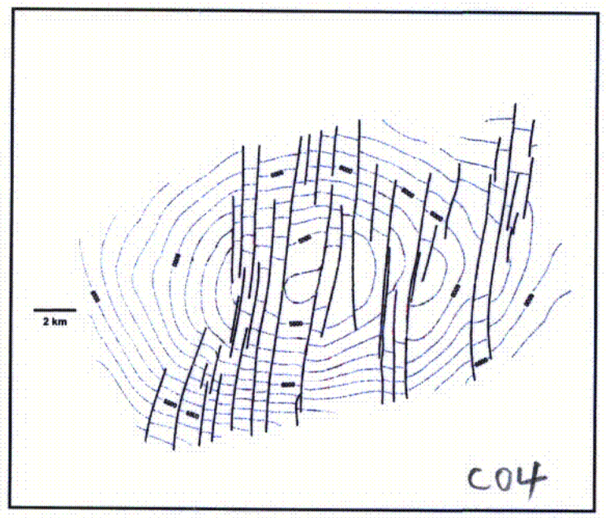

Subsurface fault trace map of offshore dome. The elliptical dome is cut by a system of parallel normal faults having strike oriented oblique to the long axis of the dome.

INFLUENCE OF REGIONAL STRAINS IN THE DEVELOPMENT OF FAULTED DOMES IN THE OFFSHORE MIDDLE EAST

Darrell W. Sims[1], David A. Ferrill[1], Alan P. Morris[2], Deborah J. Waiting[1], Futoshi Tsuneyama[3], Yoshihiko Tamura[4], and Hitoshi Okamura[3]
[1]CNWRA, Southwest Research Institute, 6220 Culebra Road, San Antonio, TX 78238-5166, USA
[2]Department of Earth and Environmental Science, University of Texas, San Antonio, TX 78249, USA
[3]Technology Research Center, Japan National Oil Corporation, Mihama-ku, Chiba 261-0025, Japan
[4]Geoscience Group Technical Department Japan Oil Development Co., Ltd., Kayabacho Tower 21-2 Shinkawa 1-Chome Chuo-ku, Tokyo 104-0033, Japan

Panel 2 of 3

Most of the structures associated with extensional faulting occur at all scales of observation in the model.

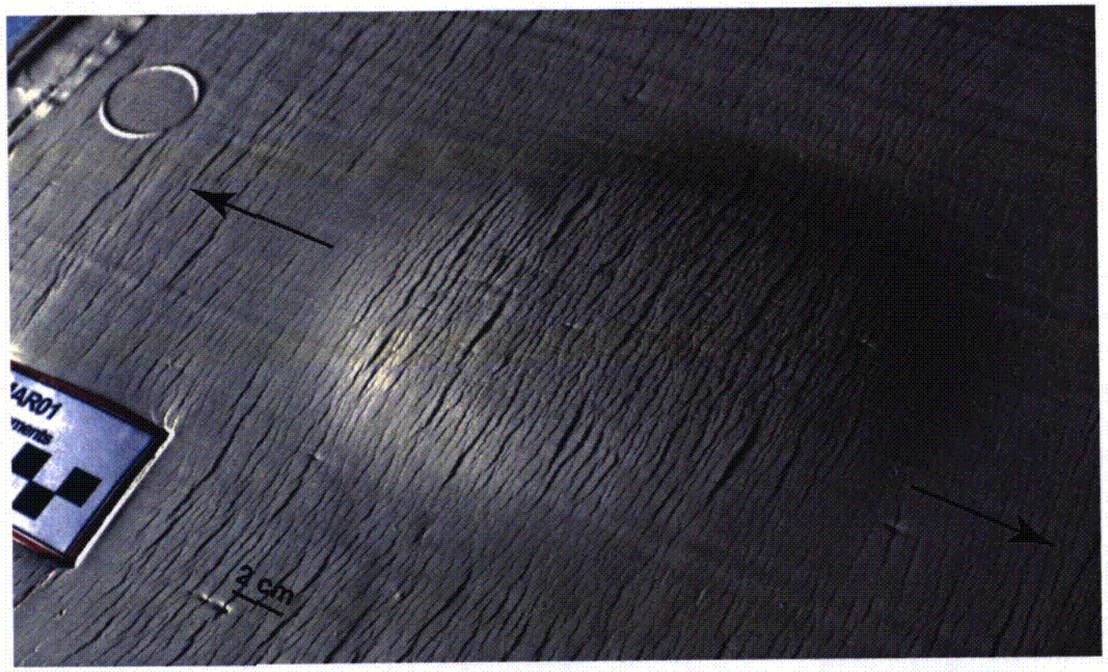

Oblique view of model 19MAR01 at end of experiment with illumination from left. Fault traces are observed to lengthen by linking of en echelon segments. Displacement transfer zones between faults exist as breached and non-breached relay ramps expressed in various geometries, including lateral curved propagation, abandoned fault and ramp segments, and newly-formed isolated fault segments.

Detail of model 19MAR01 showing displacement transfer structures at several scales.

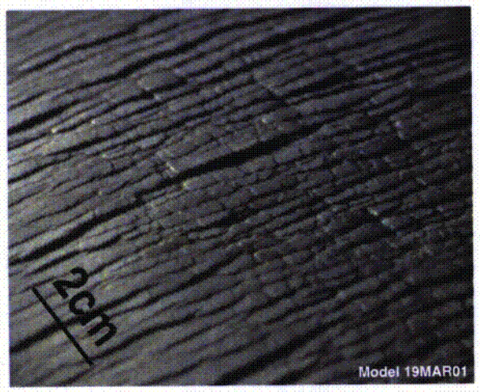

Dominant fault system oriented perpendicular to extension direction and oblique to the long axis of the dome, and showing connecting faults oriented sub-parallel with the extension direction (extension direction is approximately parallel to the scale line).

Our models indicate that the relative timing of uplift and regional extension control fault patterns, and that evolving faults and fault systems exist simultaneously at a range of sizes regardless of regional strain orientations and magnitude.

Elliptical dome formation with concurrent regional extension but without preceeding regional extension

Overview of model configuration

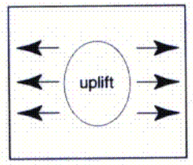

Model 19OCT00

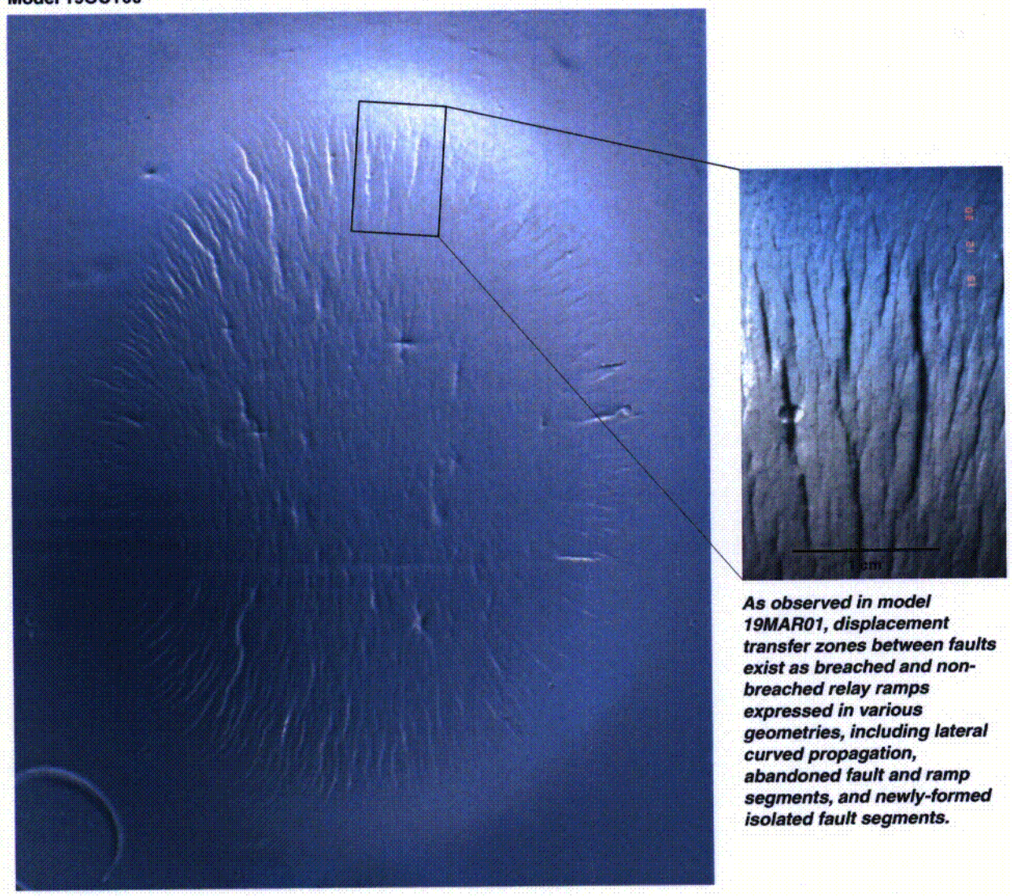

Model 19OCT00 shows elliptical dome development concurrent with (horizontal) regional extension. In comparison with model 19MAR01, the long axis of the elliptical dome is oriented perpendicular to the direction of regional extension and regional extension did not preceed doming. Note lack of fault development in areas beyond dome margin compared with model 19Mar01 (shown left) and absence of parallel faults oriented sympathetic with the direction of regional extension. The magnitude of regional extension during doming in model 3OCT00 is slightly greater (1.2x) than that of model 19MAR01. Influence of dome geometry dominates fault trace patterns producing a symmetrical radial fault pattern.

As observed in model 19MAR01, displacement transfer zones between faults exist as breached and non-breached relay ramps expressed in various geometries, including lateral curved propagation, abandoned fault and ramp segments, and newly-formed isolated fault segments.

C05

INFLUENCE OF REGIONAL STRAINS IN THE DEVELOPMENT OF FAULTED DOMES IN THE OFFSHORE MIDDLE EAST

Darrell W. Sims[1], David A. Ferrill[1], Alan P. Morris[2], Deborah J. Waiting[1], Futoshi Tsuneyama[3], Yoshihiko Tamura[4], and Hitoshi Okamura[3]
[1]CNWRA, Southwest Research Institute, 6220 Culebra Road, San Antonio, TX 78238-5166, USA
[2]Department of Earth and Environmental Science, University of Texas, San Antonio, TX 78249, USA
[3]Technology Research Center, Japan National Oil Corporation, Mihama-ku, Chiba 261-0025, Japan
[4]Geoscience Group Technical Department Japan Oil Development Co., Ltd., Kayabacho Tower 21-2 Shinkawa 1-Chome Chuo-ku, Tokyo 104-0033, Japan

Panel 3 of 3

In our models, faults initiate as isolated segments with very small trace lengths. Once faulting begins, the initiation of new small faults in the models continues until the model is halted. During this time, the number of small faults exceeds the number of large faults. The relationship between fault system size and fault density is more easily visible in model 22FEB01, regional extension without dome formation.

Regional extension, no doming

Overview of model configuration

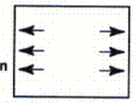

Model 22Feb01

View after 6.3 cm extension. Illumination from upper right. Faults initiate as isolated segments and are observed to grow by linking of en echelon segments.

View after 9.9 cm extension. Illumination from upper and lower right. Most of the structures associated with extensional faulting are present. Fault trace length ranges from tens of centimeters to below unaided visual detection. Displacement transfer zones between faults are expressed in various geometries, and at various scales. As faults continue to grow by segment linking, small faults continue to initiate as isolated segments.

Details of fault geometry and fault interaction in model

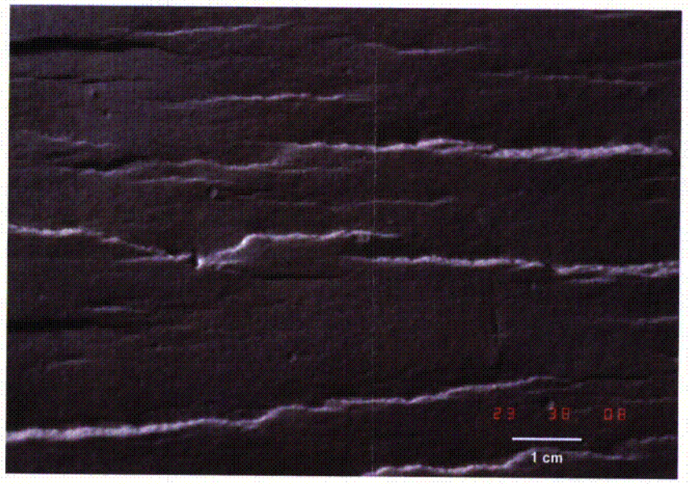

In all of our models, the populations of relatively small faults show the same patterns and geometries as the larger, clearly visible faults. Faintly visible in the images shown above and below, the number of small faults exceeds the number of relatively large faults. For example, consider the images above and below at a scale of 10cm = 1km. Most of the faults visible in the images would likely be undetectable by seismic methods. If this were a hydrocarbon reservoir, the undetectable faults would have the potential to affect reservoir compartmentalization, connectivity, permeability anisotropy, and porosity.

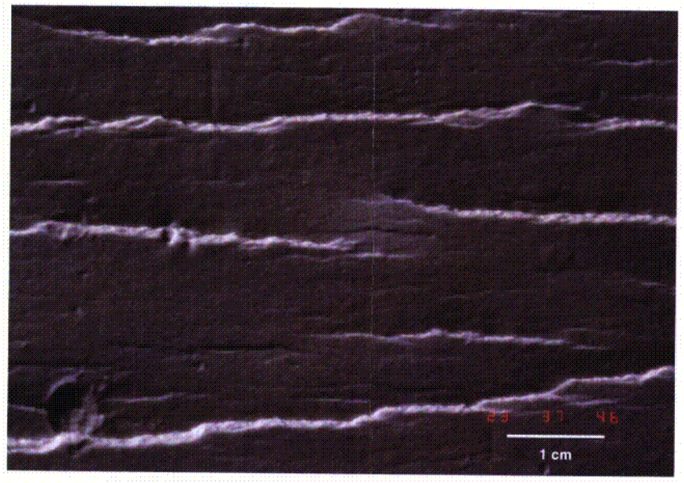

Our work demonstrates that clay cake models can be used to analyze fault development over domes in complex structural settings.

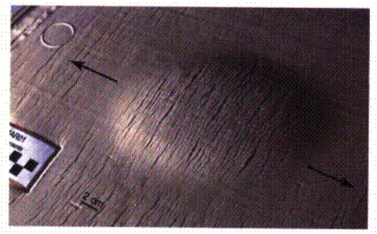

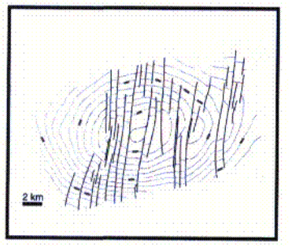

SUMMARY AND CONCLUSIONS

* **A system of parallel normal faults may dominate structural geometry over elliptical domes where dome uplift is concurrent with and possibly preceeded by regional extension.**

* **The relative timing of doming and regional extension exhibits strong control over fault patterns that form above the dome.**

* **Evolving extensional faults and fault systems exist simultaneously at a range of sizes, regardless of regional strain orientations or magnitudes.**

* **The number of small displacement faults exceeds the number of large displacement faults.**

* **In extensional systems, the number of faults existing below the resolution of seismic methods exceeds the number of faults detectable by seismic methods.**

ACKNOWLEDGMENTS
This work was funded by the Japan National Oil Corporation.

C06

ESTIMATION OF SUB-SEISMIC FAULT POPULATIONS

Alan Morris[1], David A. Ferrill[2], Yoshihiko Tamura[3], Deborah Waiting[2], Darrell Sims[2], Futoshi Tsuneyama[3], Hitoshi Okamura[3].
[1]Department of Earth and Environmental Science, University of Texas, San Antonio, TX 78249, USA
[2]CNWRA, Southwest Research Institute, 6220 Culebra Road, San Antonio, TX 78238-5166, USA
[3]Technology Research Center, Japan National Oil Corporation, Mihama-ku, Chiba 261-0025, Japan

Panel 1 of 3

ABSTRACT

In order to characterize densities of sub-seismic (<10m throw) extensional faults in carbonate rocks we mapped well-exposed normal fault systems in Cretaceous strata from 4 locations in Texas: La Cantera Parkway, and Highway 281 within the San Antonio portion of the Balcones Fault Zone, and near Balmorhea and Kent along Interstate Highway 10 in west Texas. We used outcrop mapping on photo-mosaics and scanline methods to record faults with 5 mm –10 m displacements. We calculated average extension direction, extension-parallel heave, total fault-expressed extension, and extension-parallel fault density. Maximum and minimum total fault-expressed extension were 7.91% and 0.03% respectively. Three key observations are: (1) fault density increases with total extension, (2) small-displacement faults are more numerous in areas of higher total extension, and (3) a few large faults accomplish most of the total extension. Scanlines from a 3D seismic reflection survey of faults in a carbonate reservoir exhibit lower fault density values than would be expected for the total fault-expressed extension, and the proportion of small-displacement faults is very low compared with outcrop data. This is the seismic data gap, which arises because small-displacement faults are not seismically imaged. Apparent small-displacement faults observed in seismic data are, instead, the extrapolated tips of large-displacement faults. One approach to correcting this data gap is to synthetically add faults of appropriate displacement into the seismic dataset. The basis for this correction is that total extension determines fault density, and the largest observed faults represent a large percentage of the total strain. The difference between total extension and that accommodated by observed faults is the extension deficit. Using estimates of the extension deficit, the total number of faults that should be present can be calculated. Also, the size distribution of all faults in the population can be determined using the total extension, the total number of faults and an empirical power-law relationship between fault displacement and frequency.

Figure 1

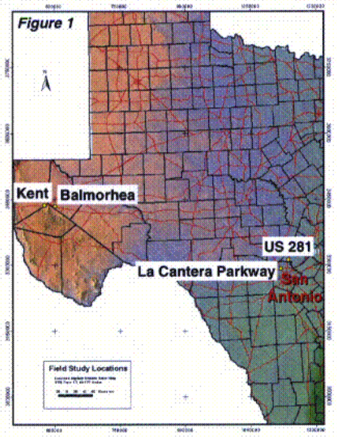

INTRODUCTION - Small faults in limestone

Outcrop maps and scanline surveys were made of well-exposed faulted Cretaceous limestone with simple extensional tectonic histories. The purpose of the field work was to evaluate frequency versus displacement relationships of sub-seismic (throw = 10 m or less) normal faults. Four locations were studied in detail to provide a database for scaling analysis of faulting in limestone (Fig. 1):

Outcrop maps

Road-cuts along La Cantera Parkway, near San Antonio, Texas (Edwards limestone).
Road cut along the south side of I-10 west of Balmorhea, Texas (Buda Formation).

Scanline surveys

Road cut along the south side of I-10 west of Kent,Texas (Boracho Formation).
Road-cuts along Highway 281, near San Antonio, Texas (Glen Rose limestone).

Geologic Sketch: West Texas

Lower Cretaceous limestone of the Buda Formation is exposed along a portion of Interstate Highway 10 west of Balmorhea, Texas. Exposed lithologies consist of bedded limestones, in part with chert nodules and arenaceous detrital material. Bed thickness varies from 30–200 cm. Tertiary age normal faults associated with southern Basin and Range extension and formation of the Rio Grande rift cut these beds.

Along interstate Highway 10, near the town of Kent, Texas, are large roadcuts in the Lower Cretaceous limestone of the Boracho Formation. Exposed lithologies consist of fine-grained thin to thick bedded limestone. Bed thickness varies from 0.5 to 2 m. Again, Tertiary age normal faults associated with southern Basin and Range extension and formation of the Rio Grande rift cut the exposed beds. Slip tendency analysis of these faults yields an intermediate principal compressive stress direction of approximately NNW-SSE which corresponds with the extension experienced by west Texas as the southern Basin and Range and Rio Grande Rift developed during Tertiary times.

Balmorhea

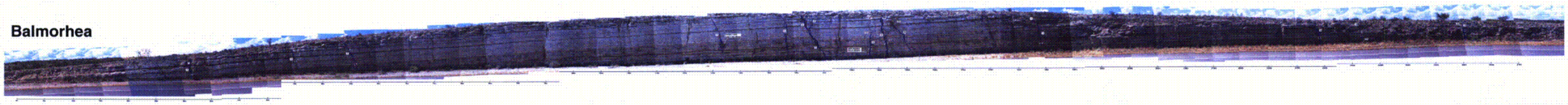

Geologic Sketch: San Antonio Area

The Balcones fault zone is a broad *en echelon* system of mostly southeast-dipping normal faults that formed during the middle to late Tertiary (Murray, 1956; Murray, 1961; Young, 1972). The 25–30 km wide fault zone trends east-northeast and spans much of central Texas. It has a maximum displacement of 366 m (Weeks, 1945), and defines the transition from flat-lying rocks of the Texas craton to gently coastward-dipping sediments of the subsiding Gulf of Mexico and related Coastal Plain. The topographic expression of the Balcones Fault zone is the Balcones escarpment, separating the Edward's Plateau to the north and west from the Texas coastal plain to the south and east. Within the Balcones fault system, the dip of strata varies from nearly horizontal to gentle coastward, with occasional localized northward dip into some faults. Growth faulting is not apparent in outcrop along the fault zone. Faulting has been interpreted as being rooted in the deeply buried foreland-basin sedimentary rocks of the Late Paleozoic Ouachita orogeny (Murray, 1956). Not all faults in the Balcones fault zone are consistent with the overall down to the southeast sense of throw and a significant number of smaller faults are antithetic to the overall trend (Collins et al., 1993; Small and Hanson, 1994; Stein and Ozuna, 1996; Collins and Hovorka, 1997; Hovorka et al., 1998; Ferrill et al., 2000). All faults are considered to have formed during the same time period and are consistent with a horizontal minimum principal compressive stress trending southeast-northwest and a vertical maximum principal compressive stress.

La Cantera Parkway, North

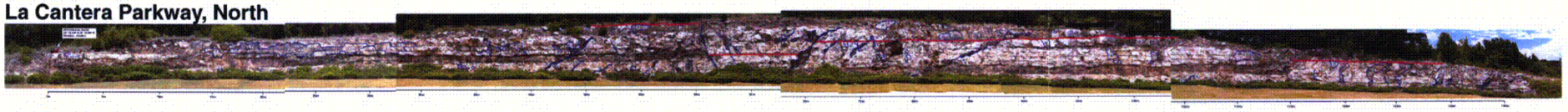

La Cantera Parkway, South

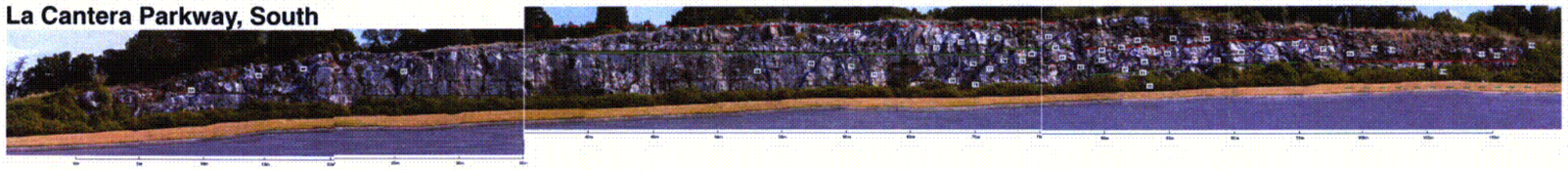

C07

Field Methods

Each roadcut was located using coordinates determined by a global positioning satellite system (GPS). For the road cut exposures along La Cantera Parkway and near Balmorhea, horizontal datum lines were surveyed and marked and the roadcuts were then photographed. The photographs were assembled into photo-mosaics of the roadcuts which were used as base maps for field measurements. Each identifiable slip surface exposed in the roadcuts was located on a photo-mosaic and measured. For each surface we recorded strike (using the right-hand-rule), dip, rake of slickenlines (where visible), displacement (parallel to slickenlines where visible, otherwise down-dip), and the maximum dip-parallel and maximum strike-parallel extent of visible fault surface. Faults were measured along bed-parallel scanlines at the Kent (550 m scanline) and Highway 281 (233 m scanline length) exposures. In all cases no faults that had displacements larger than could be determined from the exposure were encountered, and faults with displacements as small as 5 mm were resolvable.

ESTIMATION OF SUB-SEISMIC FAULT POPULATIONS

Alan Morris[1], David A. Ferrill[2], Yoshihiko Tamura[3], Deborah Waiting[2], Darrell Sims[2], Futoshi Tsuneyama[3], Hitoshi Okamura[3].
[1]Department of Earth and Environmental Science, University of Texas, San Antonio, TX 78249, USA
[2]CNWRA, Southwest Research Institute, 6220 Culebra Road, San Antonio, TX 78238-5166, USA
[3]Technology Research Center, Japan National Oil Corporation, Mihama-ku, Chiba 261-0025, Japan

Panel 2 of 3

FAULTING AS A FUNCTION OF STRAIN

Figure 2

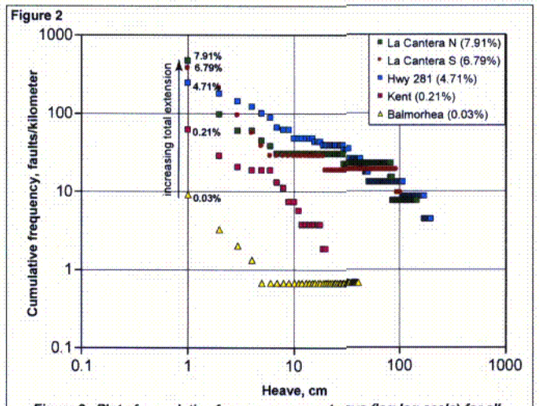

Figure 2. Plot of cumulative frequency versus heave (log-log scale) for all faults in the fault scaling study, grouped by location.

Figure 3

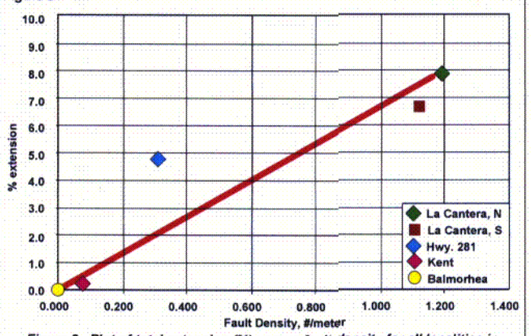

Figure 3. Plot of total extension (%) versus fault density for all localities in the scaling study.

Figure 4

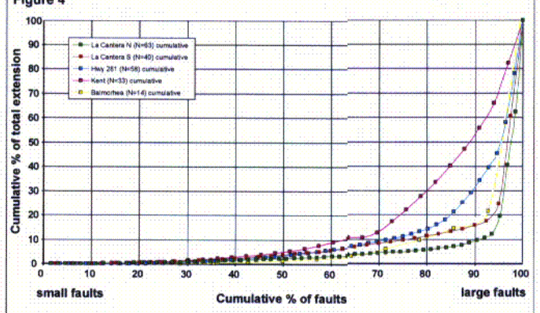

Figure 4. Plot of cumulative percent extension versus cumulative percent of faults for all faults in the scaling study, grouped by location.

Data from each location were analyzed to determine: the average extension direction, extension-parallel heave component for each fault, total extension represented by the faults, and fault density (defined as the number of faults per meter of scanline, projected parallel to the average extension direction). The data were used to plot cumulative frequency versus heave (Fig. 2), and total extension versus fault density (Fig. 3).

The relationship between strain and the distribution of each population in this plot is similar to that reported by Ackermann, et al. (2001) in their figure 7.

Small displacement faults are more numerous in areas of higher total extension (Fig. 2).

Fault density increases with increasing total extension (Fig. 3).

A relatively small portion of the total fault population contributes a large proportion of the total strain. For example, in the case of Highway 281, approximately 10% of the total extension is accommodated by 75% of the faults, and 90% of the total extension is accommodated by only 25% of the faults.

A few large faults accomplish most of the total extension.

3D SEISMIC DATA

Figure 5

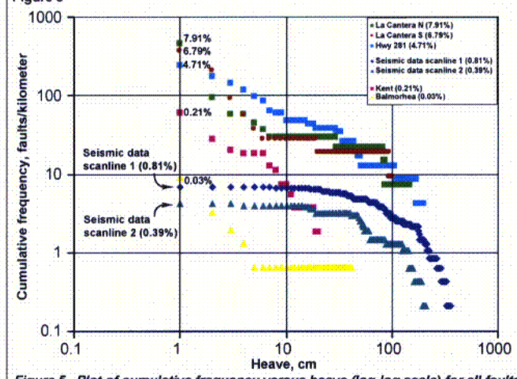

Figure 5. Plot of cumulative frequency versus heave (log-log scale) for all faults in the fault scaling study, grouped by location, including scanlines 1 and 2.

Figure 6

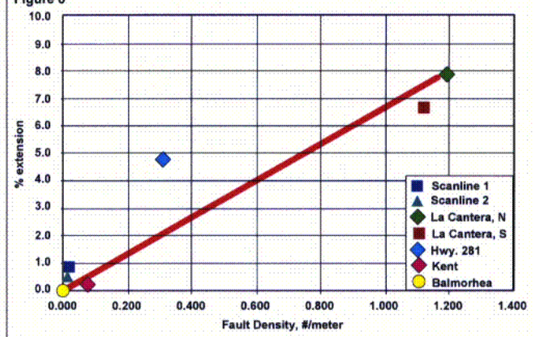

Figure 6. Plot of total extension (%) versus fault density for all localities in the scaling study, including scanlines 1 and 2.

Figure 7

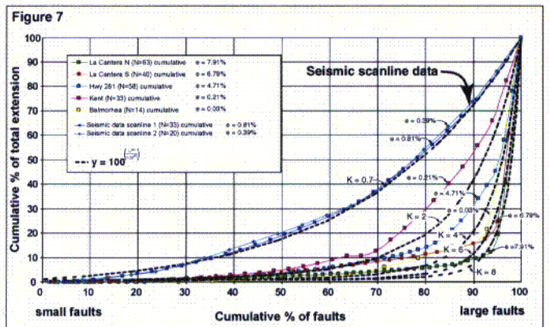

Figure 7. Plot of cumulative percent of total extension versus cumulative percent of faults for all faults in the scaling study, grouped by location, including scanlines 1 and 2. Dashed lines illustrate the form of the empirical power law relationship to describe these distributions with variable K values. Note that the seismic data plots very differently from the field data and are described by a K value of less than 1.

Scanline data extracted from a 3D seismic survey over a carbonate reservoir yield total extensions of 0.81% and 0.39% (scanlines 1 and 2 respectively).

Faults with displacement less than about 100 cm are significantly under-represented in the 3D seismic dataset (Fig. 5).

Both scanlines from the 3D seismic dataset exhibit lower fault density values than would be expected for the total extension calculated from the fault data (Fig. 6). Data from Highway 281 also show a lower fault density than might be expected, however, it plots with the other field data in Figure 4 and the lack of small faults is less marked than in the seismic dataset.

This observation is confirmed by the analysis of percent extension contributed by each section of the fault population (Fig. 7).

In comparison with the field data, there are too few small-displacement faults represented in the 3D seismic scanline datasets.

C08

The reason for the low fault density value and the paucity of small displacement faults in the seismic data is because small displacement faults are not imaged by the seismic surveys. The small displacement faults in the seismic dataset are artifacts generated by software extrapolating large, imaged, faults to a tip.

ESTIMATION OF SUB-SEISMIC FAULT POPULATIONS

Alan Morris[1], David A. Ferrill[2], Yoshihiko Tamura[3], Deborah Waiting[2], Darrell Sims[2], Futoshi Tsuneyama[3], Hitoshi Okamura[3].
[1]Department of Earth and Environmental Science, University of Texas, San Antonio, TX 78249, USA
[2]CNWRA, Southwest Research Institute, 6220 Culebra Road, San Antonio, TX 78238-5166, USA
[3]Technology Research Center, Japan National Oil Corporation, Mihama-ku, Chiba 261-0025, Japan

Panel 3 of 3

ESTIMATING SUB-SEISMIC FAULT POPULATIONS: AN EXAMPLE

Figure 8

Figure 8. Plot of total extension (%) versus fault density used to estimate fault density from % observed and estimated total extension.

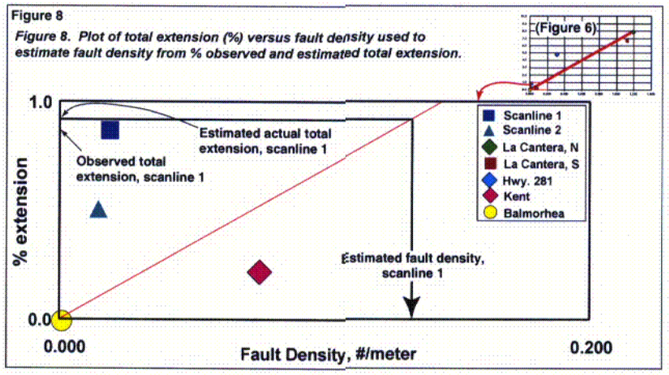

Figure 9

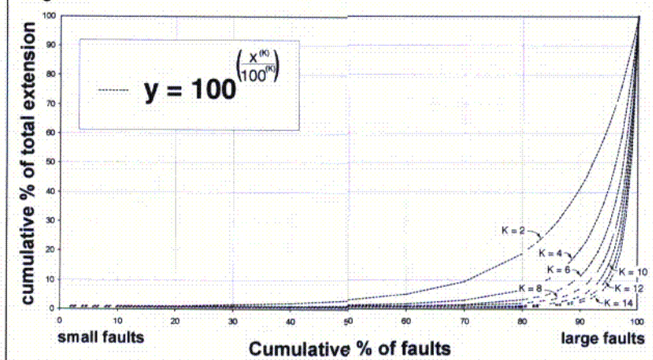

Figure 9. Empirical relationship between fault frequency and contribution to total extension.

Figure 10

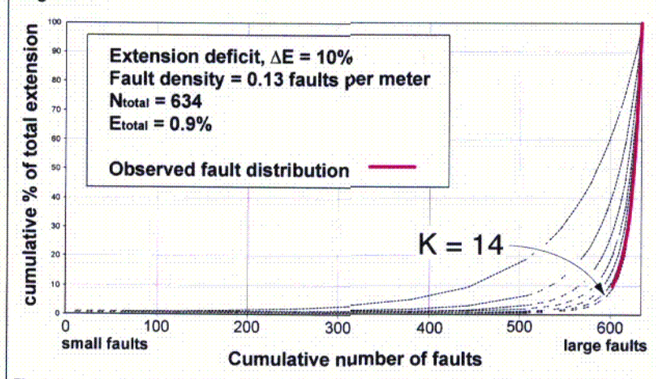

Figure 10. Estimation of sub-seismic fault population for scanline 1 where extension deficit is 10%, and the best fit K value is K = 14.

Scanline 1 from the seismic dataset contains 33 observed faults, a fault density of 0.007 faults per meter of scanline length (4714 meters) and a total observed extension of 0.81 % (Fig. 8). The observed total extension represents between 75 % and 90 %, of the actual total extension. If it represents 90 % of the actual total extension then the actual total extension will be 0.9 % (not the 0.81% observed). Using the relationship shown in Figure 6, the fault density should be 0.13 faults per meter. The total number of faults predicted to be present will be 634. Using these estimates of total extension and total number of faults, the size distribution of the total fault population can be estimated.

The empirical power-law relationship (Bonnet et al., 2001) that describes the size distribution of faults versus their contribution to total extension is shown in Figures 4 and 7. Figure 9 shows the influence of varying the value of K in this relationship.

A K value of 14 best describes the distribution of fault sizes for scanline 1.

CAVEAT

Figure 11

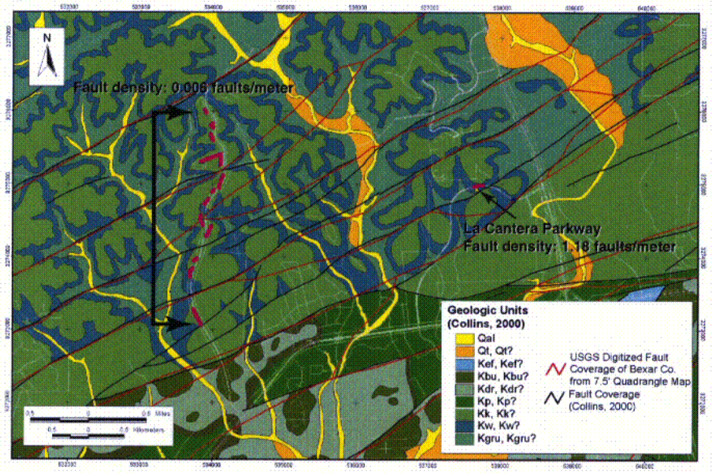

Strain is inhomogeneously distributed. The very existence of a fault is evidence of this. Using scaling, or any other strategy to populate a volume of rock with likely, but unobserved, faults is, therefore, inherently imprecise.

An example from the Balcones Fault zone, near the La Cantera Parkway exposure, illustrates how fault densities can vary over 3 orders of magnitude within similar lithologies and structural setting (Fig. 11). A total scanline length of 2 km across fault strike yields only 13 faults none with extension greater than 1 m.

Our work demonstrates that bulk strain is a determining factor of fault density and fault population characteristics. However, when attempting to estimate unobserved faults it is necessary to consider the factors that determine the distribution of strain. Such factors likely include: underlying tectonic processes (e.g., doming versus crustal extension), mechanical stratigraphy, and strain perturbations around larger faults (e.g., displacement gradient induced strains) (Ferrill and Morris, 2001).

SUMMARY AND CONCLUSIONS

(1) Fault densities are related to total strain.
(2) A small number of large faults accommodate most of the total strain.
(3) Cumulative percent extension as a function of cumulative number of faults can be described by a power law relationship.
(4) These three observations form the basis for estimating fault populations where only the largest faults in a population can be observed.
(5) Estimating unobserved fault populations from observed fault data needs to be applied with care because of the heterogeneous nature of strain.

REFERENCES

Ackermann, R.V., Schlische, R.W., Withjack, M.O., 2001. The geometric and statistical evolution of normal fault systems: an experimental study of the effects of layer thickness on scaling laws. Journal of Structural Geology, v. 23, p. 1803–1819.
Bonnet, E., Bour, O., Odling, N.E., Davy, P., Main, I., Cowie, P., Berkowitz, B., 2001. Scaling of fracture systems in geological media. Reviews of Geophysics, v. 39, p. 347–383.
Collins, E., 1993. Fracture zones between overlapping en echelon fault strands: outcrop analogs within the Balcones Fault zone, Central Texas: Gulf Coast Association of Geological Societies Transactions, v. 43, p. 77–85.
Collins, E.W., 2000. Geologic Map of the New Braunfels, Texas, 30◊60 Minute Quadrangle: Geologic Framework of an Urban-Growth Corridor along the Edwards Aquifer, South-Central Texas. The University of Texas at Austin, Bureau Economic Geology Miscellaneous, Map 39, Scale 1:100,000.
Collins, E.W., Hovorka, S.D., 1997. Structure map of the San Antonio segment of the Edwards Aquifer and Balcones Fault Zone, South-Central Texas: structural framework of a major limestone aquifer: Kinney, Uvalde, Medina, Bexar, Comal, and Hays Counties. The University of Texas at Austin, Bureau of Economic Geology Miscellaneous Map 38, scale 1:250,000.
Ferrill, D.A., Morris, A.P., 2001. Displacement gradient and deformation in normal fault systems. Journal of Structural Geology, v. 23, p. 619–638.
Ferrill, D.A., Morris, A.P., Stamatakos, J.A., Sims, D., 2000. Crossing conjugate normal faults. American Association of Petroleum Geologists Bulletin v. 84/10, 1543–1559.
Hovorka, S.D., Mace, R.E., Collins, E.W., 1998. Permeability structure of the Edwards Aquifer, South Texas—Implications for aquifer management. The University of Texas, Bureau of Economic Geology Report of Investigations 250, 55p.
Murray, G. E., 1956. Relationships of Paleozoic structures to large anomalies of coastal element of eastern North America: Gulf Coast Association of Geological Societies Transactions, v. 6, 13–24.
Murray, G. E., 1961. Geology of the Atlantic and Gulf Coastal Province of North America: New York, Harper and Brothers, 692 p.
Small, T.A., Hanson, J.A., 1994. Geologic framework and hydrogeologic characteristics of the Edwards Aquifer outcrop, Comal County, Texas. U.S. Survey Water-Resources Investigations Report 94-4117, 10p. And 1 plate (1:75,000 scale map).
Stein, W.G., Ozuna, G.B., 1996. Geological framework and hydrogeologic characteristics of the Edwards Aquifer recharge zone, Bexar County, Texas. U.S. Geological Survey Water-Resources Investigations Report 95-4030, 8p. and 1 plate (1:75,000 scale).
Weeks, A.W., 1945. Balcones, Luling, and Mexica fault zones in Texas: AAPG Bulletin, v. 29, 1733–1737.
Young, K., 1972. Mesozoic history, Llano region, in V. E., Barnes, W. C. Bell, S. E. Clabaugh, P. E. Cloud, Jr., R. V. McGehee, P. U. Rodda, and K. Young, eds., Geology of the Llano Region and Austin Area, Field Excursion: The University of Texas at Austin, Bureau of Economic Geology Guidebook 13, 154 p.

C09

ACKNOWLEDGMENTS

This work was funded by Japan National Oil Corporation. We thank H. L. McKague and B. Sagar for reviews of this presentation.